J. Membrane Biol. 55, 9–27 (1980)

The Journal of
Membrane Biology

Alamethicin-Induced Conductances in Lipid Bilayers: I. Data Analysis and Simple Steady-State Model

M. Fleischmann, C. Gabrielli*, M.T.G. Labram, A.I. McMullen and T.H. Wilmshurst**

Department of Chemistry, The University, Southampton S09 5NH, England

Summary. Conductance fluctuations induced by low concentrations of alamethicin in planar lipid bilayer membranes have been examined with a novel computer-aided analysis. A precise test is applied to show that the system is Markovian (except for the zeroth state) and an estimate is given for the (small) number of transitions between nonadjacent states: the system closely conforms to a birth-and-death process.

The complete set of rate parameters governing the steady-state distribution is derived, and it is shown that these parameters can be used to reconstruct exactly the experimental relative frequency distribution. It is also shown that the electrochemical free energies of the conductance states vary quadratically with state number for low-lying states; the free energies of activation of both the birth and death processes are linearly related to the free-energy differences between states but the transfer coefficient is close to unity. A detailed model based on the nucleation of a two-dimensional pore accounts for these observations provided both birth and death take place via an intermediate expansion of the pore lumen. This model requires two energy parameters, the "edge" and "bulk" energies of the pore, together with a trigger rate of the initial process which is a sufficient description for the steady-state behavior of this voltage-controlled system.

Ion movements through living membranes are of fundamental importance to all biological energy transduction processes such as in nerve, photoreceptor and other sensory membrane mechanisms, in drug and toxin interactions with membrane receptors, and must also be involved in many metabolic reactions carried out across membrane systems. It is possible to construct a lipid leaflet, spearating two aqueous phases, which is bimolecular in one dimension and macroscopic in the other two [16]. The behavior of these bilayers can be examined in respect of the standard *in vitro* experimental variables which is not often possible for the biomembranes they are assumed to model. In particular, the voltage-controlled ("gated") conductance channel phenomena arising from the interaction of the polypeptide alamethicin [13] with bilayers [17] may prove to be a useful model for the mechanism of nerve action. Interest in these phenomena is not due only to their being models of physiological processes; they also represent problems of electrochemical interest, e.g., the study of the very initial stages of nucleation.

Records of transmembrane currents measured at constant voltage demonstrate for bilayers doped with alamethicin [8], just as for the natural membrane in frog muscle [19], a time-series that exhibits discrete amplitudes. The form of these alamethicin-induced fluctuations between defined levels is illustrated in Fig. 1, which is taken from our own data. It may be noted that the nearly constant difference in amplitude between pairs of adjacent levels is a consequence of our choice of membrane material. Other systems [2, 5] show a more obvious amplification of the trend towards greater increments between pairs of adjacent levels at higher values of current. This observation leads directly to the supposition that alamethicin forms "multi-state" pores or cooperative channels at least. This assumption is supported by the lack of anion selectivity as well as cation *vs.* anion selectivity, the high conductivity, and the diminutive influence of membrane thickness.

* *On leave from:* Groupe de Recherches No. 4 du C.N.R.S., Physique des Liquides et Electrochimie, associé à l'Université Pierre et Marie Curie, 4, Place Jussieu, 75230 Paris, Cedex 05, France.

** Department of Electronics, The University, Southampton S09 5NH, England.

0022-2631/80/0055-0053 $03.20

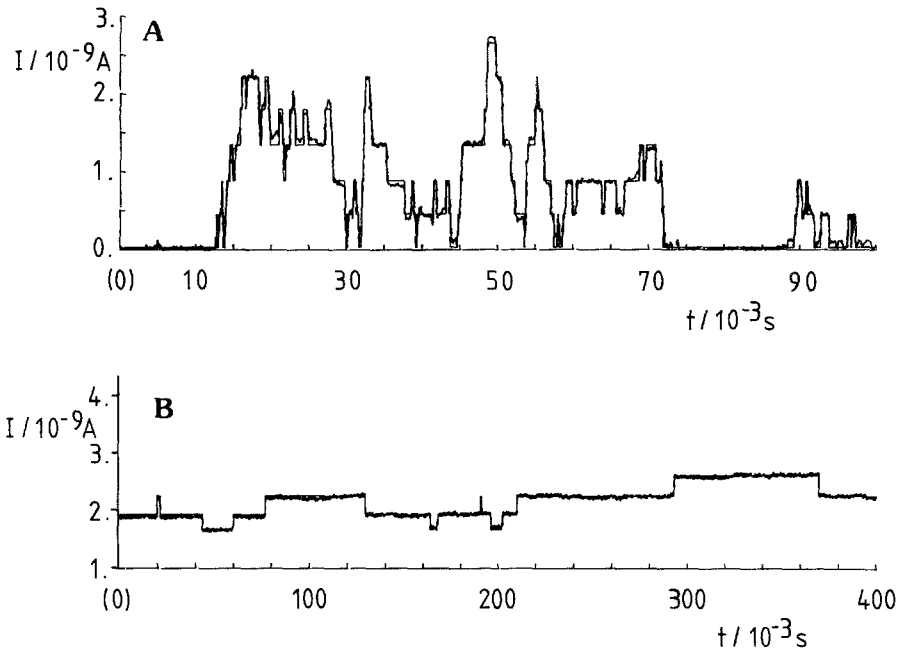

Fig. 1. Sections of current (I)-time (t) records. (A): Bilayer formed from glycerol mono-oleate (0.005 M) + cholesterol (0.01 M) in hexadecane. Potential difference, 175 mV. Membrane area $\simeq 0.4\,mm^2$. Temperature, 294 K. (B): Bilayer formed from egg lecithin (0.005 M based on mean mol wt) + cholesterol (0.01 M) in hexadecane. Potential difference, 120 mV. Membrane area $\simeq 0.4\,mm^2$. Temperature, 294 K. Aqueous phase: 2.0 M KCl + 2×10^{-8} M alamethicin RF30. The respective synchronous reclassified sequences have been overlayed (using Fig. 3 and meanstate conductances) distinguished by zero noise

Two principal detailed molecular models have been put forward for the origin of these conductance fluctuations. Gordon and Haydon [10], Hall [11], and Eisenberg, Kleinberg and Shaper [6] propose that a preformed oligomer of alamethicin molecules is inserted into the membrane with subsequent conformation changes (Boheim & Kolb [3] have also presented observations in favor of "pre-pores"); on the other hand, Baumann and Mueller [1], Smejtek [21], and Boheim [2] propose the insertion of monomers into the membrane with subsequent lateral diffusion and aggregation to form oligomers of fluctuating size (Mueller [15] has suggested a measure of "preaggregation" of monomers before insertion).

Our objectives in this first paper are twofold. Firstly, we aim to develop a computer-based analysis of the data and to establish the appropriate *stochastic* treatments whereby, without proposing any type of molecular model, a set of parameters can be defined which lead to the complete characterization of the behavior of the current fluctuations. From the data of Fig. 1, it can be seen that bursts of activity occur, on average, about every 50 msec for the mono-olein system and very much less frequently for the lecithin system, whilst durations at a given level of current between consecutive transitions may be very brief ($\sim 100\,\mu$sec) for both systems. In our view, therefore, it is essential to analyze an extremely large data-base for which only computer-based procedures remain practicable. In addition, given the ensuing statistical treatments, it seems desirable to obviate bias due to any form of preselection of data. Thus unlike previous authors, we have not at any time preselected data according to "single pore" behavior (this preselection has been based on the assumption that a single pore is active if the numbers of discernible states occurring within a single burst of current is small [5, 9], or, more specifically, if there is no deviation from the trend of greater increments in current amplitude between pairs of adjacent levels [2, 3]): in the first part of this paper we demonstrate the means by which the data can be handled in the computer subject to signal-to-noise and bandwidth restrictions; the separate validation of the premises underlying the formulation of the time-series as a birth-and-death process; the enumeration of the full set of parameters characterizing the process, and the success of this approach in a predictive capacity. An additional form of data analysis (auto-correlation and power spectral density) suitable to the study of systems for which only less complete characterizations exist is discussed briefly.

The second objective of this paper is the deduction of an appropriate kinetic model for the derived rate parameters characterizing the time-series. Concepts familiar in the field of electrochemical kinetics and especially in the field of electrocrystallization are introduced and tested as far as possible. Conclusions based on these new observations on the behavior of the system are then used to constrain further the subsequent development of a strong model governed by three identifiable quantities which permits a substantial representation of the process.

The objectives of succeeding papers will be: to derive and include corrections accounting for the contribution to the form of the time-series from the

presence of a multiplicity of pores in the membrane; to display the systematic variations of the coefficients with respect to the conductance level and with changes in the experimental variables (*cf.* Boheim [2]); to present time-dependent formulations; and to extend the application of the models to the study of biomembranes. In this latter case it is generally only possible to obtain from the data a small number of parameters, e.g., characterizing the power spectral density of the data. It is therefore essential to derive the appropriate molecular models characterized by an equally small number of parameters and to test these on model membrane systems.

Materials and Methods

Measurements to date have been made in a simple cell [18] consisting of a polytetrafluoro-ethylene (PTFE) 4-ml beaker in a perspex outer container. The beaker had a 1-mm diameter hole in a thinned wall section. Experiments on bilayers are generally accepted to be very sensitive to contamination. The cleaning procedures used in the work reported here is outlined below.

Dry glassware was rinsed with concentrated (Technical Grade) sulfuric acid and washed with distilled water followed by repeated rinsing with triple distilled water. The cell compartments were steeped in stirred 20% Decon 90 overnight, repeatedly washed as above; then left, also overnight, in a large flask of stirred triple distilled water; finally, the components were boiled in triple distilled water. This procedure for cleaning the cell was necessary because of the perspex components precluding the conventional acid treatments.

The membranes were formed by the brushed air-bubble technique [5]. Two types of membrane are reported here made with either 0.005 M 99% glycerol monooleate (Sigma Chemicals) or with 0.005 M grade 1 egg lecithin (Lipid Products, mean mol wt 756) both with 0.01 M cholesterol (BDH biochemical standard) and dissolved in 99% hexadecane (Fluka). All these were used without further purification. The hexadecane was degassed under vacuum. Solutions were made up from freshly opened ampules of the lipids and were stored for a maximum of 4 days at -5 °C under nitrogen.

Alamethicin R.F. 30 was purchased from the Microbiological Research Establishment, Porton Down, U.K. AnalaR potassium chloride was fused for 1–2 hr prior to use.

Two silver-silver chloride electrodes were used to connect the cell to the circuitry which is outlined in Fig. 2. Alamethicin was prepared as a 4×10^{-5} M solution in water (pH 9) and a single 2-µl aliquot was added to the beaker containing the positive electrode so as to make the solution 2×10^{-8} M in alamethicin with brief stirring for each new membrane.

The predetermined D.C voltages were applied to the cell via a low pass filter and currents were measured using a specially contructed transimpedance amplifier, again incorporating appropriate filters. This amplifier has a minimum rise time (10–90%) of 100 µsec with a broad band noise performance of 15 pA RMS for a capacitive source of 2500 pF (equivalent to ca. 0.4 mm^2 of membrane). Currents were recorded directly on a Racal-Thermionic Store 4D tape recorder using an FM channel (DC-5 kHz; signal/noise 48 dB). Data were simultaneously monitored on a Gould-Advance OS 4000/1 digital storage oscilloscope. This configuration allowed the continuous monitoring of the discrete fluctuations. The capacitance of the bilayer could also be estimated using the oscilloscope together with a square-wave generator.

The analog data stored on magnetic tape were passed directly through a 14-bit analog-to-digital converter (ADC) of a PDP 11-50 computer system onto disc store.

Results

Data Analysis of the Discrete Fluctuations

It is evident that data of the type shown in Fig. 1 (original record) divides naturally into a finite number of conductance states. After sampling, the second stage in the data processing is designed to allow the computer programs to assign the sampled values of the current magnitudes to the appropriate states, $\sharp_j$ ($j = 0, 1, 2, \ldots$). To achieve this, we first form the sampled frequency distribution of the current as in Fig. 3.

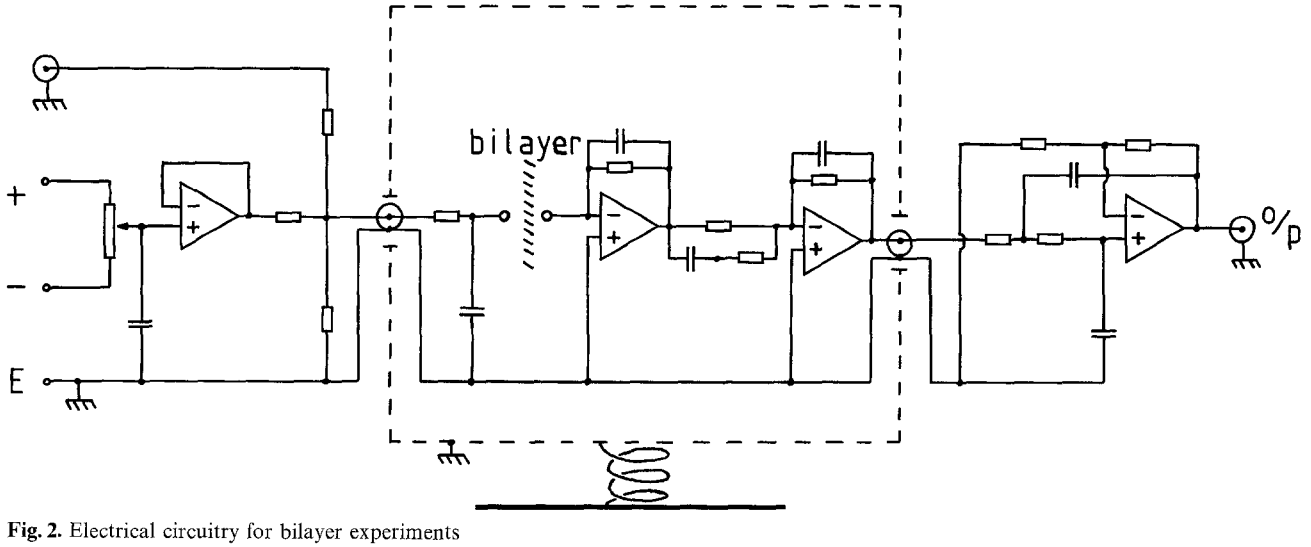

Fig. 2. Electrical circuitry for bilayer experiments

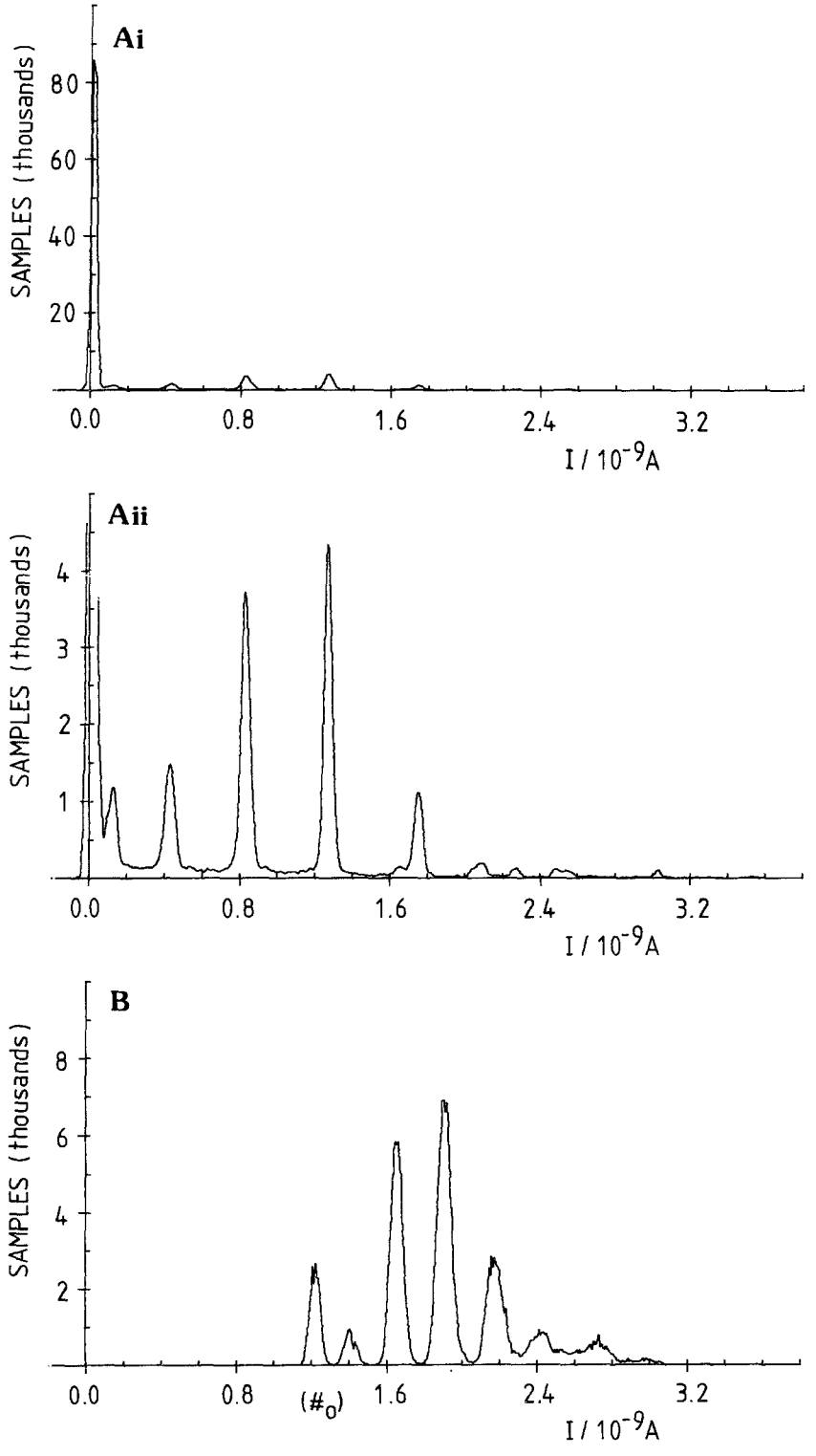

Fig. 3. Sampled frequency distributions of current (*I*). (*A*): Mono-olein system: conditions as for Fig. 1 *A*. *A ii* is an enlargement (× 20) of *A i*. (*B*): Lecithin system: conditions as for Fig. 1 *B*. The offset represents "bare" membrane leakage current. Distributions are based on 2^{18} samples evaluated at 20,000 sec^{-1} and 500 current classes

It is again evident that there are well-defined conductance states; the mid-point between peaks is the subjective choice for the upper boundary for that state of lower current. The data can now be reclassified according to these states, thereby effecting a large reduction in the disc store required.

In Fig. 1, we have overlayed the portrayed section of the original current-time record with a synchronous section obtained from the reclassified data by substituting the appropriate mean value of current, extracted as an average over the whole original data record, for the state cardinal. Figure 4 (*i*) illustrates

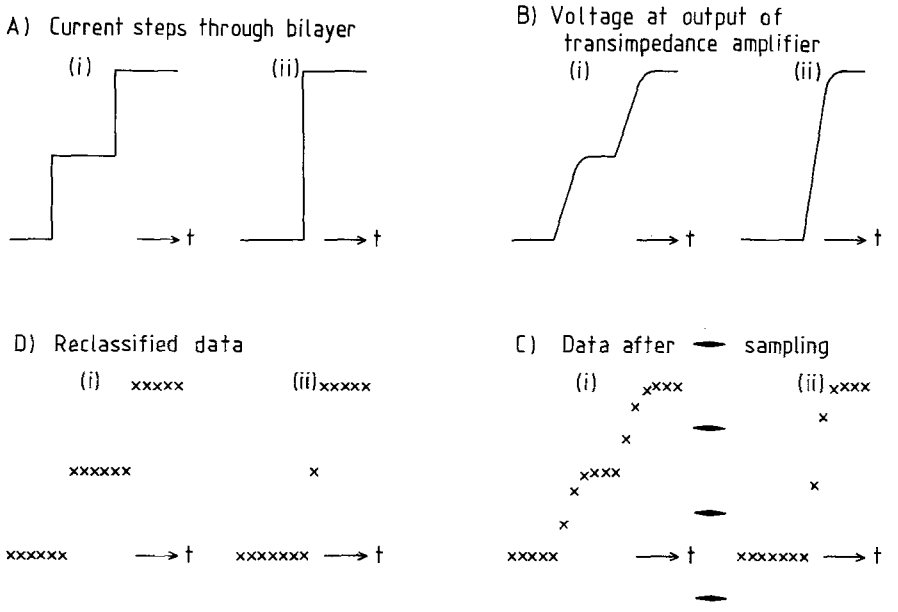

Fig. 4. Reclassification procedure. (*i*): Transitions between adjacent states. (*ii*): Transition between nonadjacent states. Note the generation of a parasitic state in this case

this procedure schematically. The further analysis of the data requires that we should characterize the nature of the process. The most important aspect, therefore, of the reclassification procedure adopted is to enable the immediate operation of the ensuing computer programmes directly on the assigned state cardinal, i.e., reclassification effects noise elimination by converting the data to a form independent of the magnitudes of the set of conductances observed.

The valid resolution of doublets and other irregularities in the sampled frequency distribution into single categories depends critically on signal-to-noise ratio of the current-sensing circuit, largely attributable to the interaction between the equivalent input noise of the amplifier employed and the capacity of the membrane investigated. But here we find it necessary to optimize the noise performance against bandwidth since the equivalent input broadband noise rises with the source capacity and with the three-halves power of bandwidth. Therefore it is of the greatest importance to reduce both the area of the bilayer and the equivalent input noise of the amplifier to their practical limits. These matters are receiving our current attention.

The compromise we have adopted at this time (a bandwidth of DC-5 kHz) leads, on the one hand, to the appearance of a number of parasitic states in the reclassified data (*see* below) for the mono-olein/cholesterol system and, on the other hand, to the grouping of doublets, etc., in the sampled frequency distribution. Two comments can be appended to this latter statement. Firstly, in choosing to study the behavior of the system at relatively low potentials, the bulk of the experimental record can be located at low conductance states, ($\sharp_0 - \sharp_5$: alamethicin initially on the positive side of the membrane [5, 9]. Moreover, seeing that for the lecithin and mono-olein systems studied here, the absolute mean-state conductances are apparently *nearly* linear functions of $\sharp_j$, the addition of conductances from more than one simultaneously existing pore (i.e., a multiplicity of pores [5]) will not invalidate the reclassification procedure. Instead, it will be shown in a later publication how this multiplicity can be accounted for in the subsequent analysis. Secondly, the resolution of the ground state into separate non- or nearly nonconducting states, although desirable in the context of prepores [2] is not practicable at present. It should be noted that $\sharp_1$ is the first obviously conductive state (subjective choice). Nevertheless, it can be seen from Fig. 1 that, subject to these restraints of resolution, reclassification maintains the salient features of the data.

The Validity of the Birth-and-Death Formulation

(*A*) *Markov Property.* The Markov property is central to the characterization and understanding of stochastic processes such as that investigated here. Instead of using the approach taken hitherto (based on an analysis of the standard histogram of durations of "dwell-times" [1]), we consider that the use of the exceedence function is more appropriate to a digitized recording. Accordingly, we have outlined the construction of such a test as follows. The Markov property is such that the evolution of the system depends only on the present and not on any previous or succeeding state.

[1] We define the dwell-time in a given state $\sharp_j$ as the duration elapsed between adjacent transitions.

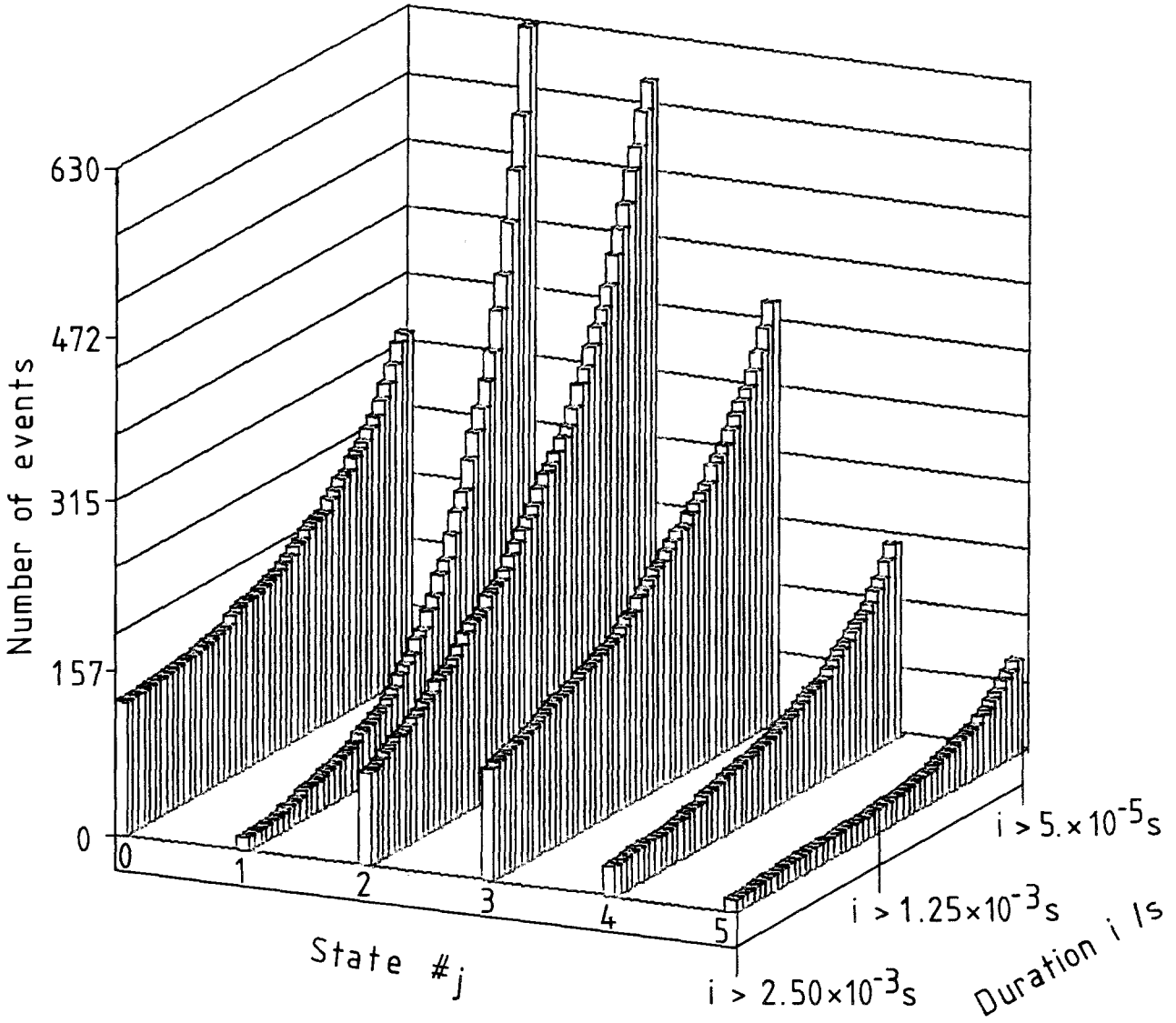

Fig. 5. Exceedance distribution of dwell-times (duration $>i$). Mono-olein system: same data as for Fig. 3*A*.

We write that the probability of the continuation of the system in a given state is independent of the length of time already spent in that state.

$$P\{T>t+x|T>t\}=P\{T>x\} \tag{1}$$

where T is the time (a random variable) and t and x are particular nonzero values [4]. It can be shown [7] that the negative exponential distribution is the only continuous distribution for a random variable which has this property.

Under the Markov hypothesis the sequence of dwell times can be regarded as N_j independent simultaneously running time intervals.
Therefore if

$P_j\{y|t>i\}$ is the probability of observing exactly y dwell-times at state $\sharp_j$ of duration *greater* than i

then

$$P_j\{y|t>i\}=\frac{N_j!(e^{-w_j i})^y\cdot(1-e^{-w_j i})^{N_j-y}}{y!(N_j-y)!} \tag{2}$$

where $w_j(s^{-1})$ is the reciprocal of the mean dwell time in $\sharp_j$. The expected value of y is given by the negative exponential distribution

$$E_j\{y\}=N_j\cdot e^{-w_j\cdot i}. \tag{3}$$

Figure 5 is a three-dimensional histogram of the

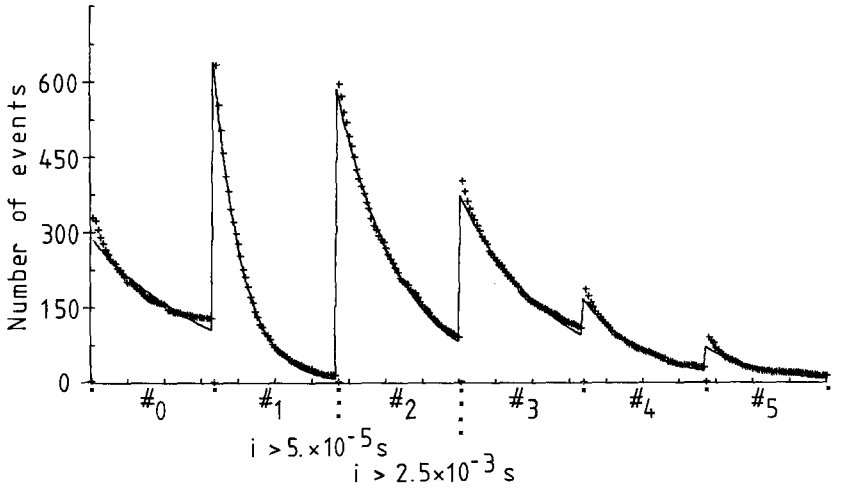

Fig. 6. Comparison of dwell-time exceedance distributions with negative exponential. Mono-olein system: same data as for Fig. 3*A*. The asterisks (*) are the observed values for the occurrences of dwell-times of duration greater than *i*, and the solid lines mark a negatively exponential function fitted to these points using the least-squares principle. Note that the independent variable *i* is reset for each curve corresponding to a separate state

Table 1. Dwell-time data: $n_j\{T>i\}=N_j\cdot\exp\{-w_j\cdot i\}$

$\sharp_j$	Mono-olein		Lecithin	
	N_j	w_j (sec^{-1})	N_j	w_j (sec^{-1})
0	290	399.9±14.7	9	–
1	639	1718.8±14.3	29	81.2± 5.3
2	585	777.5± 6.5	67	85.1± 5.7
3	372	535.3± 9.0	74	146.4±13.7
4	169	778.9±13.0	102	317.8±26.9
5	72	809.8±33.3	137	469.8±40.5

Note: $i\geqq 50\,\mu$sec (a minimum of two consecutive samples in $\sharp_j$).

frequency distribution of dwell times in $\sharp_j$ (reclassified data) having a duration greater than *i*. The data for each state can be fitted to Eq. (3) using a least-squares procedure constituting a precise test for this hypothesis. In doing this it is necessary to use correct weightings for the logarithmic transform involved but the weights must also be inversely proportional to the variance as this is a model for a Poisson process. The variance is

$$E_j\{y^2\}=e^{-w_j\cdot i}\cdot(1-e^{-w_j\cdot i}) \tag{4}$$

from which it can be seen that an iterative procedure is necessary to achieve the fit. In our analysis the shortest time defined is the interval between two consecutive data samples. The independent variable *i* is therefore conveniently expressed as the number of samples counted for a particular dwell-time, less one, the units being the reciprocal sampling rate.

It may be noted that Fig. 6 demonstrates that the conductance fluctuations do indeed largely conform to a Markov process. Table 1 lists the parameters of these curves. It follows that the time evolution of the probabilities of all the states can be derived from the recursive Chapman-Kolmogorov relation [23]. However, we note the reproducible deviation of the (first) exceedence distribution of dwell-times $\sharp_0$ from the fitted negative exponential in Fig. 6. This is the single detailed observation which cannot be fitted into a *simple* scheme of Markovian processes. This deviation coincides with the presence of a doublet in the sampled frequency distribution (Fig. 3), suggesting the complications of a subset of states and requiring suitable modifications to Eq. (2). Such an analysis, in the event of improved signal-to-noise, may lead to information pertaining to the status of the prepore and its permissible set of states. An enlargement of Fig. 6 shows that, whereas it is tempting to fit the exceedance distribution for dwell-times of higher states ($\sharp_5$ and above) as the sum of two exponentials, the distribution for $\sharp_0$ has a much smoother form. This observation is in contrast to that made by Boheim [2] on the division of the ground-state (using preselected single pore data) according to two distinct modes of behavior.

(*B*) *One-dimensional Property of the Markov Chain.* The subsidiary property defining a birth-and-death process is that transitions between nonadjacent states are forbidden. It is accepted [2, 5, 10] that such transitions are rarely observed in the available recordings of the signal. Moreover, where they do occur in these records, they are treated as a sequence of very rapid steps between adjacent states which cannot be individually resolved from the given bandwidth, i.e., the one-dimensional property is assumed. Indeed, it does seem likely that those multiple transitions occurring are merely artefacts of limited bandwidth of the transimpedance amplifier. Nevertheless, we have attempted to assess their frequency of occurrence.

In order to maximize the informational content of the reclassified data obtained from the records of

Table 2(A). Mono-olein transition data

$\sharp_j$	$n\{\sharp_j\}$	$n\{j\to j+1\}$	$n\{j+1\to j\}$	$N_j=$ $n_j\{T\geqq 0\}$	Parasitic limit $(\sharp_j)$
0	210986	336	335	335	0
1	7741	329	329	665	87
2	15982	272	272	601	19
3	16058	131	131	403	15
4	5153	55	56	187	14
5	1706	34	35	90	7
6	960	14	15	49	3
7	379	8	7	21	2
8	101	0	0	8	0

Note: Parasitic limit $(\sharp_j)=n\{j\to j+1\to j+2\}+n\{j+2\to j+1\to j\}$ with dwell-time in $\sharp_{j+1}$ represented by one or two samples only.

Table 2(B). Lecithin transition data

$\sharp_j$	$n\{\sharp_j\}$	$n\{j\to j+1\}$	$n\{j+1\to j\}$	$N_j=$ $n_j\{T\geqq 0\}$	Parasitic limit $(\sharp_j)$
0	2812	9	9	9	0
1	8649	24	23	32	0
2	65393	61	59	83	0
3	86417	55	56	117	2
4	42406	147	147	202	0
5	17793	168	168	315	0
6	14323	44	43	211	0
7	2799	2	1	45	1
8	31	0	0	2	0

Note: Parasitic limit $(\sharp_j)=n\{j\to j+1\to j+2\}+n\{j+2\to j+1\to j\}$ with dwell-time in $\sharp_{j+1}$ represented by one or two samples only.

current fluctuations, it is necessary to ensure that the restriction in bandwidth occurs within the amplifier. Provided the ADC sampling rate is set sufficiently fast compared with this bandwidth (Shannon limit), and the difference represented by the least significant "bit" is small compared to the difference between adjacent conductance-state mean values (of current), transitions between nonadjacent states will never be apparent in the reclassified data: parasitic states are interpolated in this case as a result of the reclassification procedure as illustrated in Fig. 4 (*ii*). Table 2 gives the number of samples at a given state (reclassified data), the number of transitions $n\{j\to j+1\}$ and the number of transitions $n\{j+1\to j\}$. With a sufficiently fast sampling rate to match the transimpedance amplifier response time, the number of transitions $n\{j\to j+1\}$ must therefore be equal to, or differ by one from, the number $n\{j+1\to j\}$ as required for the trajectory of such a one-step process with indeterminant origin and ending. In this paper, we have obtained the analog signal with an amplifier whose rise-time (10–90%) was 100 μsec and then sampled this at 20,000 samples per sec, i.e., the shortest time definable is 50 μsec between two consecutive samples. Column 6 of Table 2 is the sum of the numbers of transitions observed, $n\{j\to j+1\to j+2\}+n\{j+2\to j+1\to j\}$, with dwell-times at $\sharp_{j+1}$ represented by one or two samples only. This is a generous upper limit for the possible number of transitions between nonadjacent states given that a transition is faster than the response of the amplifier. (The shapes of all the transitions observed with the oscilloscope before recording on tape have been limited by the amplifier response.) It can be seen that this upper limit is both very low for the lecithin data (also indicating that the bandwidth chosen is sufficient for this system) and strongly inversely correlated to the mean-state dwell-time for the mono-olein data (*see* Fig. 5), further strengthening the assumption of this property.

(*C*) *Formulation and Comment.* Subject to our available circuitry in respect of bandwidth and signal-to-noise, we have shown that the conductance fluctuations do conform to a birth-and-death process by separately validating the two underlying premises.

There is an important simplification to the general Chapman-Kolmogorov relation for such birth-and-death processes, i.e., the set of equations

$$\frac{d}{dt}\{P_j(t)\}=\lambda_{j-1}\cdot P_{j-1}(t)+\mu_{j+1}\cdot P_{j+1}(t)$$
$$-(\lambda_j+\mu_j)\cdot P_j(t)$$
$$(j\geqq 0 \text{ and } \lambda_{-1}=\mu_0=0) \tag{5}$$

where: $P_j(t)$ is the probability of finding the system in $\sharp_j$ at time t; λ_j is the rate of birth for the transition $j\to j+1$; μ_j is the rate of death for the transition $j\to j-1$; i.e.,

$$\sharp_{j-1} \underset{\mu_j}{\overset{\lambda_{j-1}}{\rightleftharpoons}} \sharp_j \underset{\mu_{j+1}}{\overset{\lambda_j}{\rightleftharpoons}} \sharp_{j+1}.$$

Strictly speaking, these rate parameters are probability intensities and are estimated by the equations (*see* Appendix 1)

$$\lambda_j=\frac{n\{j\to j+1\}}{n\{\sharp j\}}\times\mathscr{S} \tag{6a}$$

$$\mu_j=\frac{n\{j\to j-1\}}{n\{\sharp j\}}\times\mathscr{S} \tag{6b}$$

where $\mathscr{S}$ is the sampling rate.

The P_j, λ_j and μ_j can be obtained as averages over the whole reclassified data record (loss of time-dependent information) completely independently of one another by counting the number of transitions $n\{j\to j\}$, $n\{j\to j+1\}$, $n\{j\to j-1\}$, etc. The steady-state solution for Eq. (5) is given by setting $d\{P_j(t)\}/dt=0$ so that

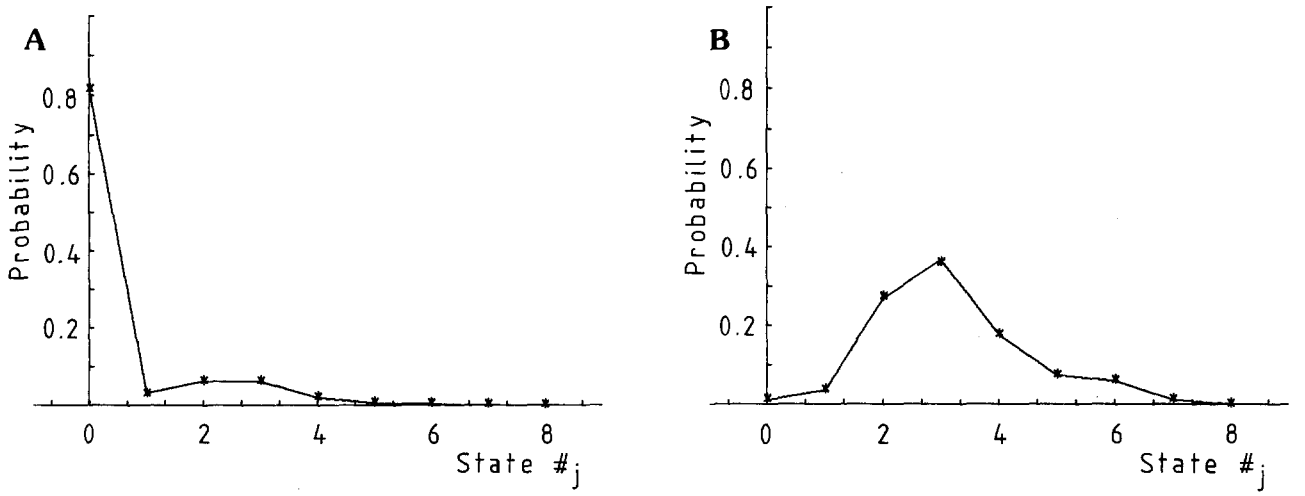

Fig. 7. Frequency distributions *vs.* calculated probability. (*A*): Mono-olein system: same data as for Fig. 3*A*. (*B*): Lecithin system: same data as for Fig. 3*B*. The asterisks (*) are the relative numbers of samples at a given state; the solid lines join the points calculated from the full set of transition parameters, λ_j and μ_j, assuming the steady state

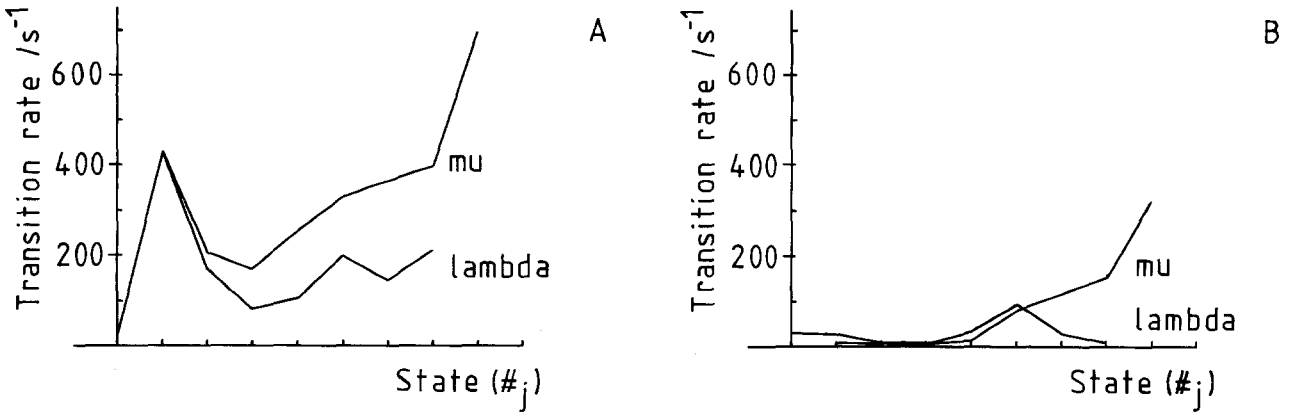

Fig. 8. Rate parameters, λ_j and μ_j, *vs.* state. (*A*): Mono-olein system: same data as for Fig. 3*A*. (*B*): Lecithin system: same data as for Fig. 3*B*. These parameters have been estimated using Eq. (6)

$$P_j^s = \pi_j \cdot P_0^s \tag{7a}$$

where

$$\pi_0 = 1 \quad \text{and} \quad \pi_j = \prod_{\varepsilon=1}^{j} \frac{\lambda_{\varepsilon-1}}{\mu_\varepsilon} \quad (j>0) \tag{7b}$$

and P_j^s is the steady-state probability of finding the system in $\sharp_j$ (at $t=\infty$). The probabilities in Eq. (7) have been normalized, i.e., obey the relation

$$\sum_{j=0} P_j^s = 1 \tag{8a}$$

so that

$$P_0^s = \left(\sum_{j=0} \pi_j\right)^{-1}. \tag{8b}$$

Figure 7 compares the observed P_j with those calculated from the observed λ_j and μ_j using the steady-state solution, Eq. (7), and demonstrates the adequacy of the set of rate parameters as a complete characterization of the data. Figure 8 is a plot of the rate parameters, λ_j, μ_j *vs.* $\sharp_j$.

The reader may wish to note that previous formulations [1–3, 5, 14, 15] have used expressions based on number concentrations of a given state (preselected data), whilst our expressions are based strictly on the probability of finding the system in a given state. Although these different forms are apparently similar, they are not strictly equivalent. In our opinion, it is important to model stochastic processes in terms of probability. Moreover, considerable confusion can arise if this policy is not adopted.

Table 3. Comparison of the reciprocal mean dwell-time, w_j, with $\lambda_j + \mu_j$

$\sharp_j$	Mono-olein		Lecithin	
	w_j	$\lambda_j+\mu_j$	w_j	$\lambda_j+\mu_j$
0	399.9	31.9	–	(64.0)
1	1717.8	1715.5	81.2	76.3
2	777.5	752.1	85.1	25.7
3	535.3	501.9	146.9	26.4
4	778.9	721.9	317.8	95.7
5	809.8	1055.1	469.8	354.1
6	–	1020.8	–	296.0
7	–	1213.7	–	321.5
8	–	1396.1	–	645.2

Note: units are $\sec^{-1}$

It is known [10] that the reciprocal of the mean dwell-time $\sharp_j$, w_j, (Eqs. (2) and (3)) is given under the Markov hypothesis by

$$w_j = \lambda_j + \mu_j. \tag{9}$$

This provides a totally independent estimate for the rate parameters (Table 3), and is analogous to Boheim's [2] consistency check for the *aggregate* validation of the premises underlying the birth-and-death formulation. The principle of the analysis could be taken further since

$$\mu_0 = 0 \Rightarrow w_0 = \lambda_0. \tag{10a}$$

Then since

$$P_1 = \frac{\lambda_0}{\mu_1} \cdot P_0 \quad \text{so } \mu_1 = \lambda_0 \cdot \frac{P_0}{P_1} \quad \text{and} \quad \lambda_1 = w_1 - \mu_1. \tag{10b}$$

Thus the w_j and P_j can be used to generate all the rate parameters separately. However, the errors are cumulative and a comparison of the *separate* rate parameters derived both in this way and from the direct counting of the transitions is inaccurate. Population sizes of all these events are limited in the data for the lecithin system, a reflection of the mean dwell-times being longer than the corresponding set for the mono-olein system; the use of more than 2^{18} samples is recommended for future investigations. Also, under the experimental conditions quoted in this paper, the state probabilities for the lecithin system drift with time (*cf.* Boheim & Kolb [3]) and it is unlikely that this system ever reaches the steady state in these experiments. However, the derivation and inclusion of modifications accounting for the contribution to the form of the time-series due to "drift" is an objective of a later publication. Therefore we have included the lecithin data in this present paper in the context of signal-to-noise and bandwidth considerations, and as a comparison to the mono-olein data.

Additional Data Analysis

If it is assumed that the process is stationary, then it is also valid to determine the properties of higher moments of the fluctuations than the mean (the first moment). In particular, the second moment is characterized by the autocorrelation function

$$\phi_I(\tau) = \lim_{T\to\infty} \frac{1}{T} \int_0^T I(t+\tau) \cdot I(t)\, dt \tag{11}$$

or by the power spectral density

$$G_I(\omega) = 4 \cdot \mathrm{Re} \int_0^\infty \exp(-\omega t \sqrt{-1}) \cdot \phi_I(\tau)\, d\tau. \tag{12}$$

Figure 9 shows a typical power spectrum. It may be noted that the "noise" is "white" at low frequencies, that only a single relaxation time can be seen, and that the high frequency asymptote shows 6dB per octave attenuation. These results may be contrasted with the data of Kolb and Boheim [12] which show evidence of two relaxations. The causes for this difference in the data is at present not clear. We note that the power spectra provide three well-defined quantities in addition to the mean value of the current, namely: the noise power at low frequency, the "corner" frequency, and the slope of the high-frequency asymptote. The interpretation of the power spectra requires the time-dependent solution of the set of Eq. (5) with appropriate boundary conditions. We will consider this elsewhere.

Interpretation

Detailed Balance Relations

We use the expressions "transient behavior of the system" or "time-evolution of the probabilities" simply to mean that there is a difference, for example, in the probability distributions to be observed immediately after the application of a potential step or at infinite time (steady state) after this stimulus – a relaxation of the probabilities. In the steady state, we would see no difference in the probabilities at different times. The steady-state solution Eq. (7) is obtained by setting the rate of change of the probabilities, $d\{P_j(t)\}/dt$, equal to zero. This implies a reflectance state (e.g., $\mu_0 = 0$) although the converse is not necessarily true. It follows that

$$\mu_j \cdot P_j^s = \lambda_{j-1} \cdot P_{j-1}^s \tag{13}$$

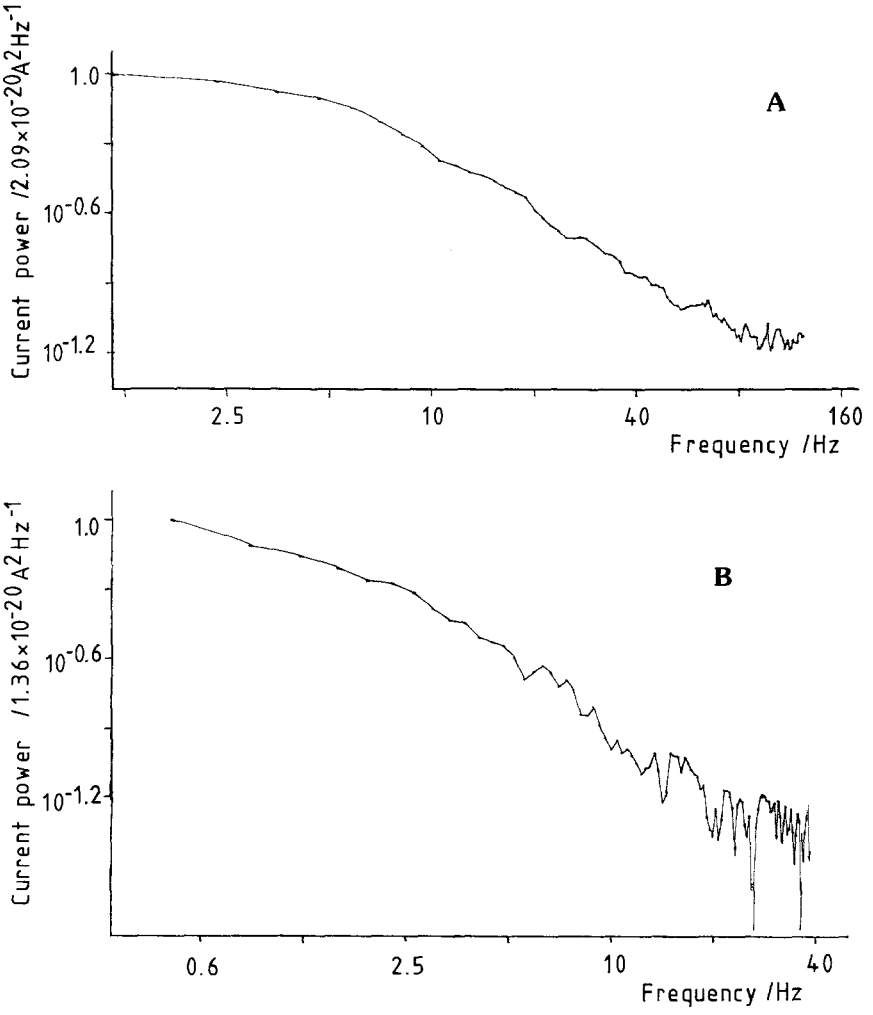

Fig. 9. Power spectral density of the current fluctuations. (*A*): Mono-olein system: same data as for Fig. 3*A*. (*B*): Lecithin system: same data as for Fig. 3*B*. It should be noted that the power spectra are "white" at low frequencies, that these define corner frequencies (corresponding to defined relaxation times), and that these demonstrate characteristic roll-offs at high frequencies $\simeq 6$ dB per octave

where P_j^s gives the probability distribution in some steady state. But this is simply a mathematical identity for a one-step process ($j \to j-1$, or $j+1$ only) since the number of transitions $n\{j \to j+1\}$ must equal the number $n\{j+1 \to j\}$. It has to be distinguished from the detailed balance relation

$$\mu_j \cdot P_j^{eq} = \lambda_{j-1} \cdot P_{j-1}^{eq} \tag{14}$$

where P_j^{eq} gives the probability distribution at thermal equilibrium [22]. However, the concept of equilibrium is very difficult to appreciate for this particular case of a voltage-controlled pore former with an ion-flux through the pore. In this analysis we have shown how the probability distribution may be reconstructed using the simple steady-state solution, Eq. (7). The averaging procedures used to calculate the sets of P_j, λ_j and μ_j over a given section of data inevitably cause the loss of any time-dependent information within this section; it is therefore unnecessary when estimating the magnitudes of λ_j and μ_j with Eq. (6) to use any analysis based on a time-dependent solution instead of Eq. (7). The time dependence of the current fluctuations may be obtained, for example, by comparing equivalent parameters from different sections of the same data (e.g., the mean recurrence time). Theoretical and experimental treatments of the time-dependence will be published later.

Interpretation of the Rate Parameters: Minimal Modelling

We now attempt to find a model for the full set of λ_j, μ_j in order to reduce this set of parameters: we proceed by making progressively stronger assumptions. Two observations can be made immediately on the functional form of the transition parameters, λ_j, μ_j, depicted in Fig. 8. Firstly it can be seen that the time series does *not* conform to a "simple" birth-and-death process for which

$$\lambda_j = j \cdot \Lambda \tag{15a}$$

$$\mu_j = j \cdot \mathrm{M} \tag{15b}$$

where Λ, M are two standard rate parameters *not* functions of j. Secondly, a set of equations such as (15), in conjunction with Eq. (5), is the natural basis for a molecular model since it contains complete information both in respect to the energy of the system and also the time-dependence. However, as discussed later, the surprising feature is that λ_j and μ_j have the same functional form, and especially that for all $j \neq 0, j_{\max}$

$$\mu_j > \lambda_j. \tag{16}$$

It will be shown that this particular observation can only be explained by a highly special model.

It is logical that the hypothetical equilibrium values of the probabilities should be governed by a distribution function which is a function of the free-energies and multiplicities of the states. This leads to

$$\frac{P_{j+1}^{eq}}{P_j^{eq}} = K \cdot \mathscr{F}(j,j+1) \cdot \exp\left\{-\frac{\bar{g}(j+1)-\bar{g}(j)}{kT}\right\}$$
$$= K \cdot \mathscr{F}(j,j+1) \cdot \exp\left\{\frac{-\Delta \bar{g}_j}{kT}\right\} \tag{17}$$

where:

P_j^{eq} is the hypothetical equilibrium probability of observing the system in $\sharp_j$; $\mathscr{F}(j,j+1)$ is a function whose form depends on the particular model chosen; K is a constant; $\bar{g}(j)$ is the electrochemical free-energy of $\sharp_j$; $\Delta \bar{g}_j$, then, is the free-energy difference driving the system from $\sharp_j$ to $\sharp_{j+1}$; k is the Boltzmann's constant; T is the absolute temperature.

In view of the detailed balance relations, we are led to assume that the steady-state is governed by a similar distribution

$$\frac{P_{j+1}^{s}}{P_j^{s}} = \frac{\lambda_j}{\mu_{j+1}} = \frac{k_\lambda}{k_\mu} \cdot \mathscr{F}(j,j+1) \cdot \exp\left\{\frac{-\Delta \bar{g}_j}{kT}\right\} \tag{18}$$

k_λ and k_μ are standard rate constants in the forward and reverse directions, respectively. In simple models k_λ will be a function of the number concentration of alamethicin, N_c (the transitions are first order in the monomer).

$$k_\lambda = N_c \cdot \vec{k} \tag{19}$$

where $\vec{k}$ is a further rate constant.[2] In common with the usual assumptions [20] made in electrochemical kinetics, we write

$$\lambda_j = k_\lambda \cdot \mathscr{F}(j) \cdot \exp\{-\alpha \cdot \Delta \bar{g}_j / kT\} \tag{20a}$$

$$\mu_{j+1} = k_\mu \cdot \mathscr{F}(j+1) \cdot \exp\{(1-\alpha) \cdot \Delta \bar{g}_j / kT\} \tag{20b}$$

where the transfer coefficient[3], α, is the fraction $(0<\alpha<1)$ of the free-energy difference driving the process in the forward direction. In these equations, $\mathscr{F}(j)$ is the number of sites at which the transition $\sharp_j$ to $\sharp_{j+1}$ can take place. For example, for a linear array of molecules on a perimeter

$$\mathscr{F}(j) = j + \delta_{o,j} \tag{21}$$

where $\delta_{o,j}$ is the Kroenecker delta function (with value unity at $j=o$ and zero elsewhere).

It has already been pointed out that the P_j may be enumerated independently from the λ_j and μ_j, so that we might determine the free-energies, $\bar{g}(j)$, and α from suitable expressions such as

$$\frac{\bar{g}(j)-\bar{g}(0)}{kT} - j \cdot \ln\left[\frac{k_\lambda}{k_\mu}\right] = \ln\left[\frac{\mathscr{F}(0) \cdot P_0^s}{\mathscr{F}(j) \cdot P_j^s}\right] \tag{22}$$

$$\alpha\left(\ln\left[\frac{\mathscr{F}(j+1) \cdot P_{j+1}^s}{\mathscr{F}(j) \cdot P_j^s}\right] - \ln\left[\frac{k_\lambda}{k_\mu}\right]\right) + \ln[k_\lambda]$$
$$= \ln\left[\frac{\lambda_j}{\mathscr{F}(j)}\right] \tag{23a}$$

$$(\alpha-1)\left(\ln\left[\frac{\mathscr{F}(j+1) \cdot P_{j+1}^s}{\mathscr{F}(j) \cdot P_j^s}\right] - \ln\left[\frac{k_\lambda}{k_\mu}\right]\right) + \ln[k_\mu]$$
$$= \ln\left[\frac{\mu_{j+1}}{\mathscr{F}(j+1)}\right] \tag{23b}$$

with $\mathscr{F}(j)$ given by Eq. (21).

Figure (10) is a plot of $\ln(P_0/j \cdot P_j]$ against $\sharp_j$. The figure shows a least-squares fit to the expression

$$\bar{g}(j) = A \cdot j^2 + B \cdot j + C \qquad (j = 1, \ldots, 5) \tag{24}$$

and it can be seen that $\bar{g}(j)$ is a parabolic function of j at least for small j.

Figure 11 is a plot of an equation ((32) using a special version of the model) directly comparable to (23a). The analysis has been based on 3 million data points and covers the first 18 observable states (no preselection of single pore data). It is satisfying that the plot is indeed straight, substantiating the simple assumptions made in formulating Eq. (20), and that the slope of the line is 1.07 so that $\alpha = 1$ is a suitable estimate. The points which deviate strongly (but not systematically) from the line are for the high states

[2] Equation (19) has been written in the most simple form. The reaction order may well be different from unity: concentration effects are not examined in this paper.

[3] The factor α defined here is not the same as that used by Boheim [2]. Our usage follows the standard practice in electrochemical kinetics.

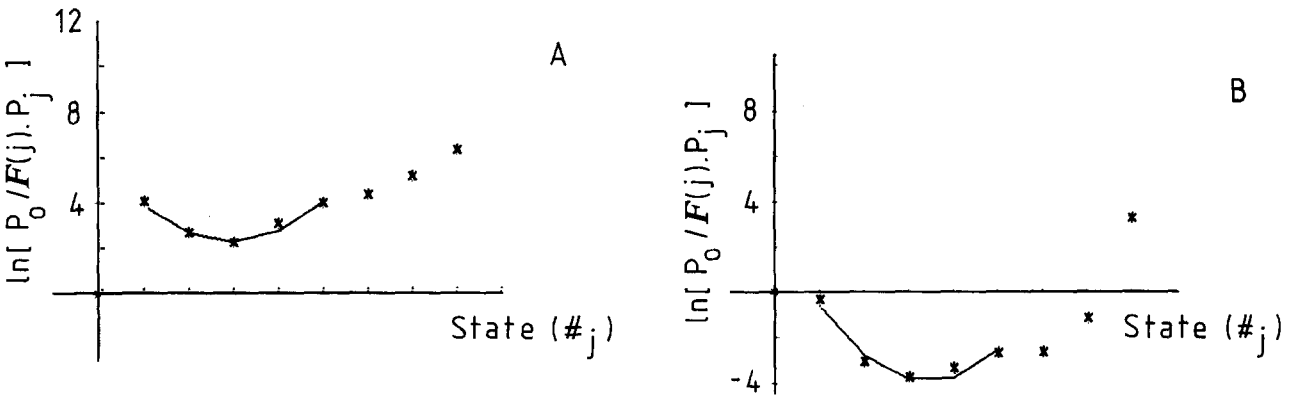

Fig. 10. Free-energy (Eqs. (21) and (22)) *vs.* state. (*A*): Mono-olein system: same data as for Fig. 3*A*. (*B*): Lecithin system: same data as for Fig. 3*B*. The solid lines mark a quadratic function fitted to the observed values (*) using the least squares principle

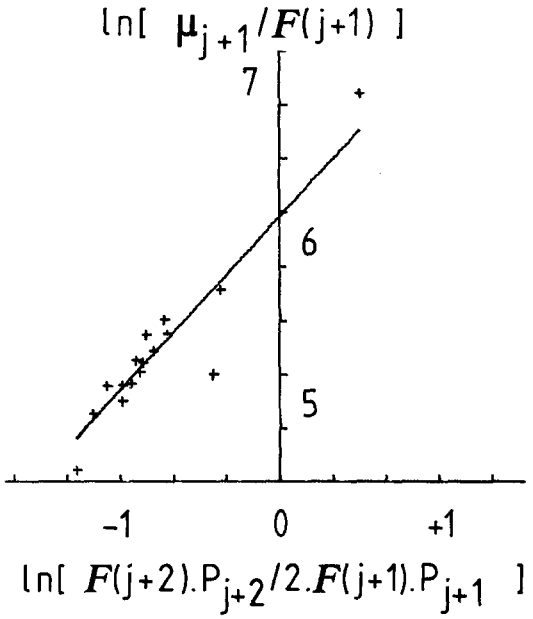

Fig. 11. Transfer coefficient, α: linear fraction of the free-energy differences (Eqs. (21) and (32). Mono-olein system: data includes data of Fig. 3*A* but with data-base extended to 3.2^{20} samples (20,000 sec^{-1}). Note that the points deviating from the fitted line ($\alpha \simeq 1.07$) most strongly in the left-hand quadrant are given by $j = 15, 16, 17$. The point in the right-hand quadrant is given by $j = 0$

for which the population of observed events is insufficient even using such a very large data base.

Detailed Model

Any detailed molecular model must explain that the electrochemical free energy for $\sharp_j$ follows Eq. (24)[4]. Here we restrict attention to one model which after further modification explains this variation and all our other observations on the reclassified data base. According to the initial form of this model, molecules of alamethicin are successively inserted into the membrane at the periphery of a "cylindrical" pore, Fig. (12*a*). The free-energy of such a pore is defined by a minimum of two terms (*see* Appendix 2):

(1) "edge" energy, σ, per molecule of alamethicin at the periphery (in units of kT);

(2) "bulk" energy, ψ, proportional to the energy for replacing membrane lipid by electrolyte (water) per water molecule (in units of kT).

Hence $\Delta\bar{g}_j$ contains a constant edge-energy moiety together with a bulk-energy moiety, the latter being proportional to the change in cross-sectional area of the pore. In this way we obtain

$$\Delta\bar{g}_j \approx (j+1)^2 \cdot \psi - j^2 \cdot \psi + \sigma = (2j+1)\psi + \sigma \qquad (25)$$

which is consistent with Eq. (24).

This model is related to those used in the theory of two-dimensional nucleation except that here we are considering the formation of a hole lined by pore-forming molecules. However, there is a fundamental difference in these two areas: the form of the frequency distribution, Fig. (3), shows that ψ must be positive (i.e., the exclusion of water from the membrane is a spontaneous process) whereas σ is negative (i.e., the insertion of the pore-former into the membrane is a spontaneous process). Indeed, the observation of a steady state in the fluctuations demands that ψ be positive. The signs of these energy terms are precisely opposite to those for nucleation (*see* Appendix 3).

It will be seen from Fig. 12 that the number of sites at which the transition $\sharp_j$ to $\sharp_{j+1}$ can take place is $(j+\delta_{o,j})$ while there are $(j+1)$ sites for the reverse

[4] We note that Boheim [2], also, has shown that the difference, $\Delta\bar{g}_j$, is proportional to j (our notation).

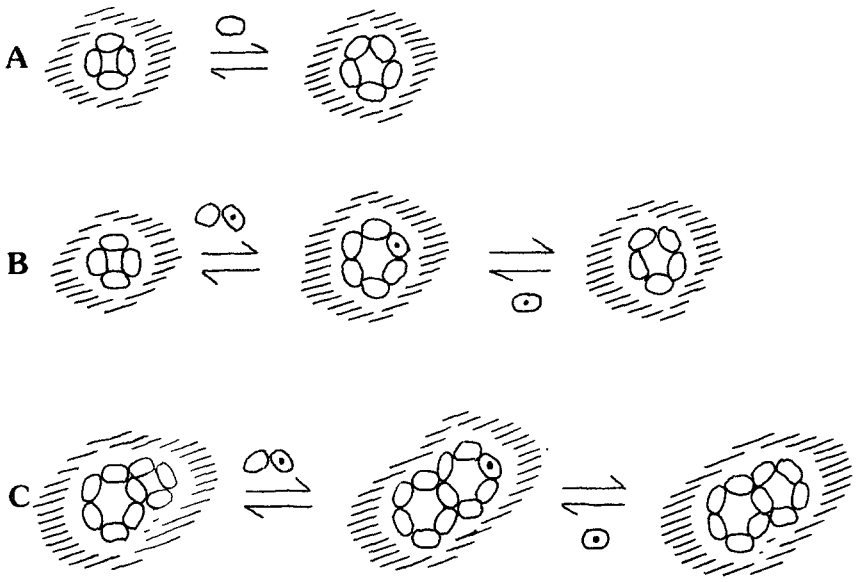

Fig. 12. Models of pore-expansion. (*a*): Insertion of a monomer (alamethicin) [1, 15]. (*b*): Insertion of a dimer (alamethicin/alamethicin or lipid). (*c*): Dimer expansion with additive structures

transition. We therefore find for λ_j and μ_{j+1}, retaining the factor α,

$$\lambda_j = \mathscr{F}(j) \cdot k_\lambda \cdot \exp\{-\alpha(2j+1)\psi - \alpha\sigma\} \tag{26a}$$

$$\mu_{j+1} = \mathscr{F}(j+1) \cdot k_\mu \cdot \exp\{(1-\alpha)(2j+1)\psi + (1-\alpha)\sigma\} \tag{26b}$$

which are identical to Eq. (20) with $\Delta\bar{g}_j$ given by Eq. (25). Hence

$$\ln\left[\frac{\lambda_j}{\mathscr{F}(j)}\right] = -2\alpha\psi \cdot j - \alpha(\psi+\sigma) + \ln[k_\lambda] \tag{27a}$$

$$\ln\left[\frac{\mu_{j+1}}{\mathscr{F}(j+1)}\right] = 2(1-\alpha)\psi \cdot j + (1-\alpha)(\psi+\sigma) + \ln[k_\mu] \tag{27b}$$

whilst

$$\ln\left[\frac{P_j^s}{P_0^s}\right] = \ln\left[\prod_{\varepsilon=1}^{j} \frac{\lambda_{\varepsilon-1}}{\mu_\varepsilon}\right] \quad (j>0)$$
$$= -\psi \cdot j^2 + (\ln[k_\lambda/k_\mu] - \sigma) \cdot j - \ln[j]. \tag{28}$$

However, it is apparent that Eq. (26) is inconsistent with the observation that the reverse transition parameters have the *same* functional form (*see* Eq. (16)) as those in the forward direction as functions of state since $0<\alpha<1$. This restraint can only be accounted for by assuming a modification to the distribution function (18) incorporating an intermediate state, $\sharp_j \rightleftharpoons \sharp_I \rightleftharpoons \sharp_{j+1}$. A model consistent with our results is based on a "pre-equilibrium" between states j and I, the second step being rate determining. We obtain firstly

$$\frac{P_{j+1}^s}{P_j^s} = \frac{k_\lambda}{k_\mu} \cdot \mathscr{F}(j, I, j+1) \cdot \exp\left\{-\frac{\bar{g}(I) - \bar{g}(j)}{kT}\right\} \cdot \exp\left\{-\frac{\bar{g}(j+1) - \bar{g}(I)}{kT}\right\}$$
$$= \frac{k_\lambda}{k_\mu} \cdot \mathscr{F}(j, I, j+1) \cdot \exp\left\{\frac{-\Delta\bar{g}(j)}{kT}\right\} \tag{29}$$

with I denoting the intermediate state, and assuming that the transition, $\sharp_{j+1} \rightarrow \sharp_I$, also involves an expansion of the pore. For convenience, we take this intermediate state to be the next higher state, $\sharp_{j+2}$. Figure (12*b*) represents the modified form of the model, i.e., the insertion of an alamethicin dimer followed by exclusion of one of these two molecules from the structure ($\mathscr{F}(I)=2$). It must be noted, however, that the expansion of the ring could also be due to the insertion of nearest lipid neighbors, together with the alamethicin moiety, followed by slow exclusion of this lipid. Secondly, if the steps $I \rightarrow j+1$ and $j+1 \rightarrow I$ are rate determining,

$$\lambda_j = 2 \cdot \mathscr{F}(j) \cdot k_\lambda \cdot \exp\{-(2j+1)\psi - \sigma\} \cdot \exp\{-\alpha(2j+3)\psi - \alpha\sigma\} \tag{30a}$$

$$\mu_{j+1} = \mathscr{F}(j+1) \cdot k_\mu \cdot \exp\{-\alpha(2j+3)\psi - \alpha\sigma\} \tag{30b}$$

$$\frac{\bar{g}(j) - \bar{g}(0)}{kT} - j \cdot \ln\left(\frac{k_\lambda}{k_\mu}\right) - j \cdot \ln[2] = \ln\left(\frac{\mathscr{F}(0) \cdot P_0^s}{\mathscr{F}(j) \cdot P_j^s}\right) \tag{31}$$

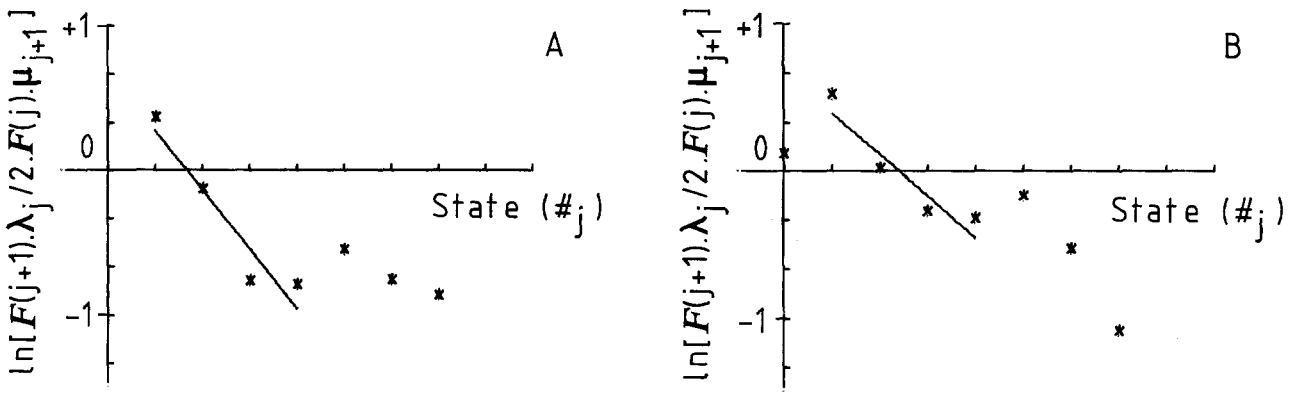

Fig. 13. 3 parameter model: determination of values (Eqs. (21) and (33). (*A*): Mono-olein system: same data as for Fig. 3*A*. *Note:* $\ln[\lambda_0/2\mu_1]$ is to be found at -4.005. (*B*): Lecithin system: same data as for Fig. 3*B*. The solid lines mark a straight line fitted to the observed (*) values using the least-squares principle

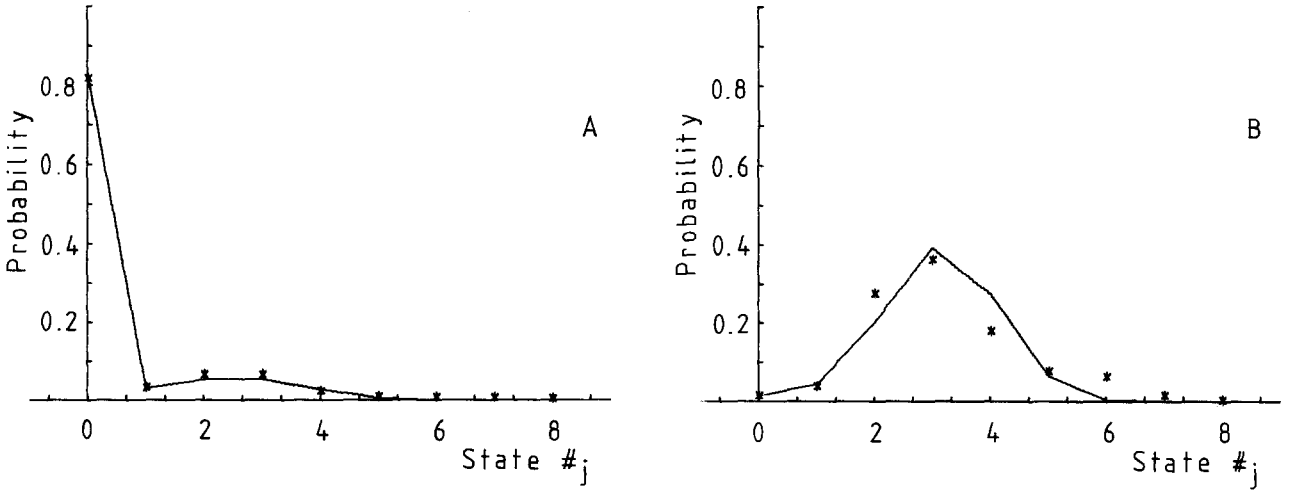

Fig. 14. Frequency distribution *vs.* calculated probability. (*A*): Mono-olein system: same data as for Fig. 3*A*. (*B*): Lecithin system: same data as for Fig. 3*B*. The asterisks (*) are the relative numbers of samples at a given state; the solid lines join the points calculated on the steady-state model (Eq. (34)) with values for the 3 parameters derived from the data

$$\alpha\left(\ln\left[\frac{\mathscr{F}(j+2)\cdot P^s_{j+2}}{2\cdot\mathscr{F}(j+1)\cdot P^s_{j+1}}\right]-\ln\left[\frac{k_\lambda}{k_\mu}\right]\right)+\ln[k_\mu]$$
$$=\ln\left[\frac{\mu_{j+1}}{\mathscr{F}(j+1)}\right]. \qquad (32)$$

Figure (10) is not affected by this modification, (22) → (31), whilst k_μ also becomes a function of the number concentration (19). Rearranging

$$\ln\left[\frac{\mathscr{F}(j+1)\cdot\lambda_j}{2\cdot\mathscr{F}(j)\cdot\mu_{j+1}}\right]=-2\psi\cdot j-\psi+(\ln[k_\lambda/k_\mu]-\sigma). \qquad (33)$$

Figure (13) is a plot of $\ln[2(j+\delta_{o,j})\cdot\lambda_j/(j+1)\mu_{j+1}]$ against $\sharp_j$. Note the special value of λ_o/μ_1 and the complicated structure at higher states. The intermediate points have been fitted by a straight line giving appropriate values of ψ and $(\ln[k_\lambda/k_\mu]-\sigma)$ listed in Table 4. The steady-state solution for the model is given by

Table 4. Observed values for the 3-parameter model

	Mono-olein	Lecithin
ψ	0.4107	0.5686
$\ln[k_\lambda/k_\mu]-\sigma$	1.7909	3.2156
λ_0/μ_1	0.0368	3.0758

$$\frac{P^s_j}{P^s_0}=\phi\cdot 2^j\cdot\frac{1}{j}\cdot\exp\{j\cdot(\ln[k_\lambda/k_\mu]-\sigma)-j^2\cdot\psi\} \qquad (j>0) \qquad (34)$$

where ϕ=(the observed value of λ_o/μ_1)/$2\exp\{(\ln[k_\lambda/k_\mu]-\sigma)-\psi)$ and the normalizing conditions $\Sigma_{j=o}P_j=1$ giving P_o. It may be noted that $\mathscr{F}(0)=1$ together with ϕ represents the trigger rate of

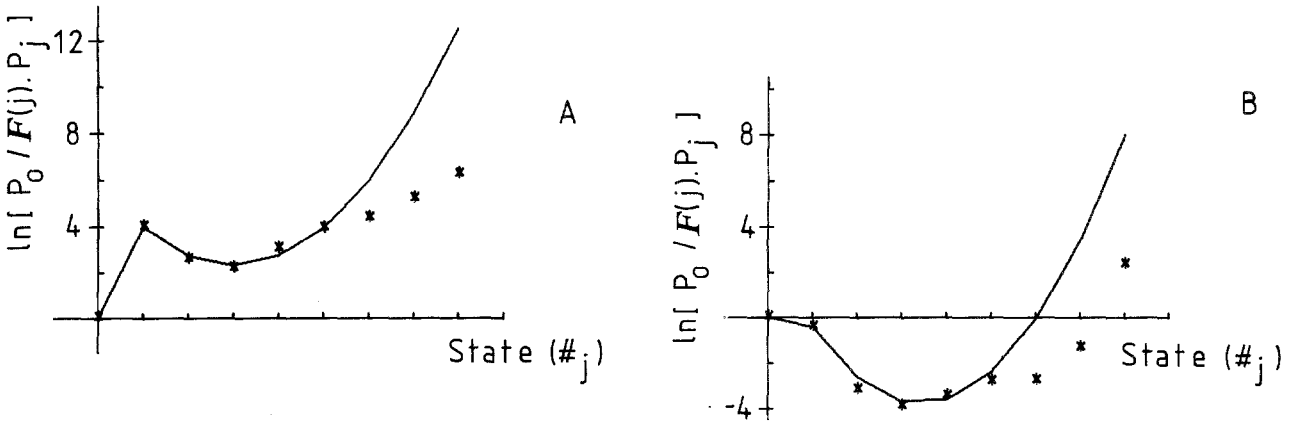

Fig. 15. Free-energy (Eqs. (21) and (34)) *vs.* state. (*A*): Mono-olein system: same data as for Fig. 3*A*. (*B*): Lecithin system: same data as for Fig. 3*B*. The asterisks (*) are the observed values; the solid lines join the points calculated on the steady-state model (Eq. (34)) with values for the 3 parameters derived from the data

the first conducting state. A comparison similar to that given in Fig. 7 can then be made (Fig. 14). A comparison for the function $\frac{\bar{g}(j)-\bar{g}(o)}{kT}$ is also given in Fig. 15.

Discussion

It has been shown that the principal features of the experimental data for alamethicin-induced transitions in mono-olein (and lecithin) membranes can be accounted for by a simple model based on an electrochemical kinetic treatment of nucleation. This model predicts the transition rates using only two energy parameters (bulk and edge) and the trigger rate of the first conducting state. The plots demonstrating the fit of the model, Figs. 14 and 15, indicate a deviation at higher conductance states, however. Careful inspection of the sampled frequency distribution (Fig. 3) reveals that the peaks at higher conductance have a more complex structure than those at lower conductance (one is completely divided) consistent with more than one pore being active; this is more obvious in the data of Eisenberg et al. [5] where the incremental conductances are far less uniform. The analysis of extended data bases recorded from highly active bilayers in which high states are apparent indicate a more complex structure than that due to a single quadratic equation (24), also supporting the likelihood of several simultaneously-active pores. The high probability of observing zero conductance with the mono-olein system (due to "death" of pores) coupled with the relatively low probability of observing the first state suggests that a second pore could be additive as in Fig. 12*c* rather than independent.

A further deviation noted in our preceding treatment of the Markov property is that the transition $\sharp_0$ to $\sharp_1$ is not Markovian. Inspection of Fig. 3 shows that the distribution at $\sharp_0$ also has a complex structure which could well be due to the superposition of two states as would be found if the absolute first state (i.e., before reclassification) were essentially nonconducting. Such a superposition could lead to the observed deviation from Markovian behavior (superposition of two exponentials). Yet this possibility alone would still be insufficient to account for the approximately cubic form of the probability distribution for the mono-olein system showing that the transition $\sharp_0 \rightarrow \sharp_1$ has a special character which we have expressed by the parameter ϕ in our treatment. We conclude that a better model should replace $\lambda_o(\phi, \delta_{o,j})$ by some Poisson process triggering the subsequent birth and death process (with absorption at $\sharp_0$).

The energy parameters, ψ and σ, must depend on the applied potential and, it is their change with potential which accounts for the gating action in turn caused by pore-formation. The two free-energy terms used in this model can, in principle, be completely and separately determined from the data, and it is evident that the alamethicin system therefore affords a sensitive probe of membrane properties.

It has already been pointed out that the expansion of the pore is governed by a positive bulk energy term, ψ, and a negative edge energy term, σ (the signs of these terms must be in the opposite sense to those found in nucleation - *see* Appendix 3). These signs predict that the form of the pore will be elliptical (in the plane of the membrane) rather than circular, depending on their ratio (*cf.* refs. [6, 9]).

It should be noted that any information as to changes in the structure of the pore with increasing

size which would be revealed by changes in the spacing of the current levels has been set aside in this analysis by virtue of the reclassification procedure.

Clearly, power spectral densities of current fluctuations through membranes promise an improved understanding of the pertinent transport processes. However, as emphasized earlier, the apparent simplicity of such data – a single relaxation – requires very careful interpretation: alamethicin-induced fluctuations in the current through lipid bilayers are demonstrably more complex than this simplicity in the power spectrum would suggest, seeing that each pore fluctuates between at least five identifiable states. The possibility of similar complexity in the energetics of sodium and potassium channels in biomembranes can scarcely be ignored. In this context it is indeed fortunate that, not only can the kinetics of a model system be completely evaluated, but also contained in an expression sufficiently simple to encourage the identification between detailed molecular mechanisms and the characteristics of the power spectra which they generate.

Appendix 1

Evaluation of the Transition Parameters, λ_j and μ_j

The transition parameters are defined by

$$p\{j+1, t+\Delta t/j, t\} = \lambda_j \cdot \Delta t + O(\Delta t)^2 \tag{A1}$$

$$p\{j-1, t+\Delta t/j, t\} = \mu_j \cdot \Delta t + O(\Delta t)^2. \tag{A2}$$

Moreover,

$$p\{j+1, t+\Delta t/j, t\} = p\{j+1, t+\Delta t \text{ and } j, t\}/p\{j, t\} \tag{A3}$$

$$p\{j-1, t+\Delta t/j, t\} = p\{j-1, t+\Delta t \text{ and } j, t\}/p\{j, t\}. \tag{A4}$$

Therefore, by counting

(i) $n\{\sharp_j\}$, the number of samples in $\sharp_j$

(ii) $n\{j \to j+1\}$, the number of transitions (j, t) to $(j+1, t+\Delta t)$

(iii) $n\{j \to j-1\}$, the number of transitions (j, t) to $(j-1, t+\Delta t)$

so that

$$p\{j+1, t+\Delta t \text{ and } j, t\} = n\{j \to j+1\} / \sum_{j=0} n\{\sharp_j\} \tag{A5}$$

$$p\{j, t\} = n\{\sharp_j\} / \sum_{j=0} n\{\sharp_j\}. \tag{A6}$$

Then

$$p\{j+1, t+\Delta t/j, t\} = n\{j \to j+1\}/n\{\sharp_j\} \tag{A7}$$

and

$$\lambda_j = \frac{1}{\Delta t} \cdot n\{j \to j+1\}/n\{\sharp_j\}. \tag{A8}$$

Likewise

$$\mu_j = \frac{1}{\Delta t} \cdot n\{j \to j-1\}/n\{\sharp_j\}. \tag{A9}$$

In evaluating λ_j and μ_j, $\frac{1}{\Delta t}$ can be identified with the sampling rate $\mathscr{S}$.

Appendix 2

As an alternative to the statement of the energies ψ and σ, the following derivation may be preferred. We consider a hollow cylinder of n alamethicin molecules bridging the membrane with electrolyte (mainly water) in its lumen. Then the length of this cylindrical pore, the thickness of the membrane, is given by h and, its circumference is given by $n \cdot a$ where a is the short dimension of each alamethicin molecule at the interfacial perimeter. We take χ to be the free-energy for replacing membrane by water per water molecule (of volume v) and ξ to be the free-energy of the edge interaction in the sandwich electrolyte/alamethicin/membrane per unit area. Then the volume of the pore is $n^2 a^2 h/4\pi$ and the surface area exposed to membrane is $n a h$. The free-energy of the pore is given by

$$\bar{g}(n) - \bar{g}(o) = \frac{n^2 a^2 h}{4\pi v} \cdot \chi + n a h \cdot \xi. \tag{A10}$$

For simplicity, we choose

$$\psi = \frac{a^2 h}{4\pi v \cdot kT} \cdot \chi \tag{A11}$$

$$\sigma = \frac{a h}{kT} \cdot \xi \tag{A12}$$

so that

$$\bar{g}(n) - \bar{g}(o) = (n^2 \psi + n\sigma) \cdot kT. \tag{A13}$$

Notice, however, that to a first approximation

$$\chi = \gamma \cdot v/h \tag{A14}$$

where γ is the surface energy of the water/lipid/water interphase. γ will depend on the applied potential; χ will not follow Eq. (A14) exactly because the electric field will be distorted in the region of the pore.

Appendix 3

Using the notation of Appendix 2, the conventional view would be that $\chi<0$ and $\xi>0$ so that, as a function of n, $\bar{g}(n)-\bar{g}(o)$ reaches a metastable maximum for some n, n^*. Spontaneous growth of the center will then take place since, although

$$n\,a\,h\,\xi>\frac{n^2a^2h}{4\pi v}|\chi| \ldots n<n^* \tag{A15}$$

yet

$$n\,a\,h\,\xi<\frac{n^2a^2h}{4\pi v}|\chi| \ldots n>n^* \tag{A16}$$

n^* is given by

$$\frac{d\bar{g}(n)}{dn}=O=n^*\cdot\frac{a^2h}{2\pi v}\cdot\chi+a\,h\cdot\xi \tag{A17}$$

$$\therefore n^*=-\frac{2\pi v}{a}\cdot\frac{\xi}{\chi}. \tag{A18}$$

So, with the usual signs of χ and ξ, Eq. (A16) shows that there can be no stable bilayer!

Glossary of Symbols

- $\sharp_j$ The j^{th} state of the system, $j\geqq 0$.
- $P_j(t)$ The probability of finding the system in $\sharp_j$ at time t.
- P_j^s The steady-state probability of finding the system in $\sharp_j$, $t=\infty$.
- P_j^{eq} The hypothetical equilibrium probability of finding the system in $\sharp_j$.
- P_j The observed relative frequency for the system being in $\sharp_j$, an average taken over the considered section of data.
- w_j The reciprocal of the mean dwell-time in $\sharp_j$, Eq. (3); (sec^{-1}).
- N_j The calculated total number of dwell-times in $\sharp_j$ for the considered section of data, Eq. (3).
- λ_j The rate of birth for the transition $j\to j+1$, Eq. (6a); (sec^{-1}).
- μ_j The rate of death for the transition $j\to j-1$, Eq. (6b); (sec^{-1}).
- $\mathscr{S}$ The sampling rate, 20,000 for the data given in this paper; (sec^{-1}).
- $I(t)$ The instantaneous current at time t; (A).
- $\phi_I(\tau)$ The current autocorrelation function, Eq. (11); (A^2).
- $G_I(\omega)$ The current power spectral density, Eq. (12); $(A^2\,\text{Hz}^{-1})$.
- $\bar{g}(j)$ The electrochemical free energy of $\sharp_j$; (J).
- $\Delta\bar{g}_j$ The change in electrochemical free energy for the transition $\sharp_j$ to $\sharp_{j+1}$.
- $\mathscr{F}(j)$ A frequency factor representing a multiplicity in transitions between states.
- k Boltzmann's constant; $1.38\times10^{-23}JK^{-1}$.
- T Absolute temperature, 294 K for the data given in this paper.
- K A constant.
- k_λ A standard rate constant in the forwards direction of increasing state; (sec^{-1}).
- k_μ A standard rate constant in the reverse direction of decreasing state; (sec^{-1}).
- N_c Number concentration of alamethicin units at the bilayer/electrolyte interface; (dm^{-3}).
- $\vec{k}$ A standard rate constant in the forwards direction of increasing state independent of the number concentration N_c; $(dm^3\,sec^{-1})$.
- α Linear fraction of the free-energy difference, $\Delta\bar{g}_j$.
- $\delta_{0,j}$ Kroenecker delta: unity if $j=0$ and zero elsewhere.
- ψ "Bulk" free-energy of replacing membrane lipid by electrolyte, Eq. (25) and Appendix 2; dimensionless.
- σ "Edge" free energy of interaction electrolyte/alamethicin/membrane lipid, Eq. (25) and Appendix 2; dimensionless.
- h The length of a cylindrical pore: thickness of the membrane; (m).
- a The short dimension of an alamethicin molecule, at the interfacial perimeter; (m).
- v The volume of a water molecule; (m^3).
- χ The free-energy for replacing membrane by water per unit molecule, Appendix 2; $(J\,\text{m}^{-3})$.
- ξ The free energy of the edge interaction in the sandwich electrolyte/alamethicin/membrane per unit area of pore exposed to membrane, Appendix 2; $(J\,\text{m}^{-2})$.
- n^* Critical size of a nucleus.
- γ The surface energy of the water/lipid/water interphase; $(J\,\text{m}^{-2})$.

References

1. Baumann, G., Mueller, P. 1974. A molecular model of membrane excitability. *J. Supramol. Struct.* **2**:538
2. Boheim, G. 1974. Statistical analysis of alamethicin channels in black lipid membranes. *J. Membrane Biol.* **19**:277
3. Boheim, G., Kolb, H.A. 1978. Analysis of the multi-pore system of alamethicin in a lipid membrane. I. Voltage jump current-relaxation measurements. *J. Membrane Biol.* **38**:99
4. Cooper, R.B. 1972. Introduction to queuing theory. MacMillan, New York
5. Eisenberg, M., Hall, J.E., Mead, C.A. 1973. The nature of the voltage-dependent conductance induced by alamethicin in black lipid membranes. *J. Membrane Biol.* **14**:143
6. Eisenberg, M., Kleinberg, M.E., Shaper, H.J. 1977. Channels across black lipid membranes. *Ann. N.Y. Acad. Sci. (in press)*
7. Feller, W. 1968. An introduction to probability theory and its applications. Vol. I. (3rd ed.) Wiley, New York
8. Gordon, L.G.M., Haydon, D.A. 1972. The unit conductance channel of alamethicin. *Biochim. Biophys. Acta* **255**:1014
9. Gordon, L.G.M., Haydon, D.A. 1975. Potential dependent conductances in lipid membranes containing alamethicin. *Phil. Trans. R. Soc. (London) B* **270**:433
10. Gordon, L.G.M., Haydon, D.A. 1976. Kinetics and stability of alamethicin conducting channels in lipid bilayers. *Biochim. Biophys. Acta* **436**:541
11. Hall, J.E. 1975. Toward a molecular understanding of excitability. *Biophys. J.* **15**:934
12. Kolb, H.A., Boheim, G. 1978. Analysis of the multi-pore system of alamethicin in a lipid membrane. II. Autocorrelation analysis and power spectral density. *J. Membrane Biol.* **38**:151
13. Martin, D.R., Williams, R.J.P. 1976. Chemical nature and sequence of alamethicin. *Biochem. J.* **153**:181
14. Moore, L.E., Neher, E. 1976. Fluctuation and relaxation analysis of monoazomycin-induced conductance in black lipid membranes. *J. Membrane Biol.* **27**:347
15. Mueller, P. 1976. Membrane excitation through voltage-induced aggregation of channel precursors. *Ann. N.Y. Acad. Sci.* **264**:247

16. Mueller, P., Rudin, D.O., Ti Tien, H., Westcott, W.L. 1962. Reconstitution of cell membrane structure *in vitro* and its transformation into an excitable system. *Nature (London)* **192**:979
17. Mueller, P., Rudin, D.O. 1967. Action potentials induced in biomolecular lipid membranes. *Nature (London)* **217**:713
18. Mueller, P., Rudin, D.O. 1970. Bimolecular lipid membranes: Techniques of formation, study of electrical properties, and induction of ionic gating phenomena. *In:* Laboratory techniques in membrane biophysics. H. Passow and R. Stamfli, editors. p. 141. Springer-Verlag, New York
19. Neher, E., Sakmann, B. 1976. Single-channel currents recorded from membrane of denervated frog nuscle fibres. *Nature (London)* **260**:799
20. Parsons, R. 1954. Equilibrium properties of electrified interphases. *In:* Modern aspects of electrochemistry. J. O'M Bockris and B.E. Conway, editors. Vol. 1. Butterworths, London
21. Smejtek, P. 1974. Simple model of ion transport through alamethicin channels in lipid membranes. *Chem. Phys. Lipids* **13**:141
22. Van Kampen, N.G. 1976. The expansion of the master equation. *In:* Advances in Chemical Physics. I. Prigogine and S.A. Rice, editors. Vol. 34, p. 245. Wiley, New York
23. Whittle, P. 1970. Probability. Penguin Books, Harmondsworth, Middlesex

Received 25 April 1979; revised 28 September 1979